(1) The assumption that the thermal conductivity can be expressed as a sum of the two contributions, K_L due to longitudinal phonons and K_T due to transverse phonons, is valid for Mg_2Sn. The change of slope in the phonon conductivity versus temperature, which occurs at about 80°K, can be explained by the present approach of two-mode conduction (first proposed by Holland for Si and Ge, and later used by us for InSb, GaAs, and Si-Ge alloys[11]).

(2) It has been shown that almost all the heat transport at high temperatures is by transverse phonons.

(3) In order to account for the observed magnitude of phonon conductivity, especially near the maximum, one has to consider the resonant scattering of phonons by bound donor electrons. The elastic scattering part of the second-Born-perturbation results of Kwok's theory alone accounts for the observed values of the phonon conductivity near the maximum.

[11] C. M. Bhandari and G. S. Verma, Phys. Rev. **138**, A288 (1965); **140**, A2101 (1965).

ACKNOWLEDGMENTS

This work was supported by the University Grants Commission of India. The authors are grateful to Professor K. S. Singwi, Professor Vachaspati, Professor B. Dayal, and Dr. M. M. Joshi for their interest.

PHYSICAL REVIEW B VOLUME 1, NUMBER 2 15 JANUARY 1970

Nonrelativistic Energy-Band Structure of Au†*

HERBERT SCHLOSSER
Department of Physics, Cleveland State University, Cleveland, Ohio 44115
(Received 30 July 1969)

The composite wave variational method has been utilized to determine the electronic band structure, Fermi surface, and Fermi energy of Au in the nonrelativistic approximation. The crystal potential utilized in these calculations was constructed from Liberman, Waber, and Cromer's numerical Hartree-Fock solutions of the Dirac equation for the Au atom, including crystal exchange in the Slater $\rho^{1/3}$ approximation. Comparison is made with Shoenberg's experimental determination of Fermi-surface parameters using the de Haas–van Alphen effect.

I. INTRODUCTION

THE work reported here is an application of the composite wave variational method[1,2] (CWV) to calculation of the energy-band structure of gold. This marks the first application of this technique to an investigation of the band structure of a heavy element. The previous applications of this method have been to calculations of the band structure of the light alkalis,[1] x-ray scattering factors, and charge densities for Li,[3] and to positron annihilation in the alkalis.[4]

In Ref. 1 (SM), we presented several variational principles for the energy which apply to trial wave functions which are discontinuous on a surface within a unit cell in the crystal.[5] These expressions, which are at the heart of the CWV method, lead directly to the various forms for the matrix elements and secular equation given in SM. They also lead directly to the rapidly convergent iterative procedure for solving the secular equation which is a major advantage of the CWV method,[6] and which is discussed in detail in Sec. II 4 of SM.

In this calculation we make use of a crystal potential which was constructed by superposing Liberman, Waber, and Cromer's[7] numerical Hartree-Fock solutions of the Dirac equation for gold, including a crystal exchange contribution in the Slater $\rho^{1/3}$ approximation.[8] The energy bands have been plotted out in a number of symmetry directions and also $E(\mathbf{k})$ has been calculated at a large number of general points. This has enabled a precise determination of the Fermi surface. Comparison is made with Shoenberg's[9] experimental determination of Fermi-surface parameters using the de Haas–van Alphen effect.

† Supported in part by U. S. Army Research Office (Durham), under Contract No. DA-31-124-ARO-D-307.
* The bulk of this research was performed at the Polytechnic Institute of Brooklyn, Brooklyn, N. Y. 11201.
[1] H. Schlosser and P. M. Marcus, Phys. Rev. **131**, 2529 (1963).
[2] Preliminary results reported at Chicago APS Meeting, Bull. Am. Phys. Soc. **13**, 57 (1968).
[3] E. Jensen and H. Schlosser, Bull. Am. Phys. Soc. **12**, 485 (1967).
[4] H. Schlosser, Bull. Am. Phys. Soc. **13**, 644 (1968).
[5] The application of the variational principle for discontinuous wave functions (SM) to semiempirical molecular calculations has been suggested by R. G. Parr (private communication), while T. Loucks [Phys. Rev. **139**, A231 (1965)] has obtained matrix elements for a relativistic APW scheme from a generalization of the variational principles of (SM).
[6] It should be pointed out that Loucks (Ref. 5) has not made optimal use of the variational principle for discontinuous wave functions in his relativistic calculations since he does not take advantage of the iterative procedure, described in Ref. 1, for solving the secular equation.
[7] D. Liberman, J. T. Waber, and D. T. Cromer, Phys. Rev. **137**, A27 (1965).
[8] J. C. Slater, Phys. Rev. **81**, 385 (1951).
[9] D. Shoenberg, Phil. Trans. Roy. Soc. (London) **A225**, 85 (1962).

II. COMPOSITE WAVE VARIATIONAL METHOD

The CWV method for solving the energy-band problem in solids is discussed in detail in SM.[1] We will now briefly summarize the major points of the development of this method, restricting ourselves for simplicity to simple monatomic Bravais lattices.[10]

We wish to solve Schrödinger's equation,[11]

$$\mathbf{H}\psi(\mathbf{r})=[-\nabla^2+V(\mathbf{r})]\psi(\mathbf{r})=\epsilon\psi(\mathbf{r}), \tag{1}$$

in the crystal, given the one-electron potential energy function $V(\mathbf{r})$. Since the potential $V(\mathbf{r})$ has lattice periodicity, i.e., $V(\mathbf{r}+\mathbf{R}_l)=V(\mathbf{r})$, where $\mathbf{R}_l$ is any translation vector of the space lattice, we may apply periodic boundary conditions on the crystal and restrict ourselves to finding solutions of (1) in a single primitive cell subject to the appropriate cellular boundary conditions.[1] This is equivalent to seeking Bloch-type solutions

$$\psi(\mathbf{r},\mathbf{k})=e^{i\mathbf{k}\cdot\mathbf{r}}u_{\mathbf{k}}(\mathbf{r}), \tag{2a}$$

where

$$u_{\mathbf{k}}(\mathbf{r}+\mathbf{R}_l)=u_{\mathbf{k}}(\mathbf{r}) \tag{2b}$$

and $\mathbf{r}$ is in the first Wigner-Seitz cell, while $\mathbf{k}$ is in the first Brillouin zone. It is well known that near the nucleus the wave function, $\psi(\mathbf{r},\mathbf{k})$, has atomiclike character, with many oscillations, while near the cell boundaries it is well represented by an expansion in a few plane waves. But the spherical wave expansion, appropriate near the nucleus, cannot satisfy the cellular boundary conditions: Hence, as discussed in Sec. II 2 of SM, one is led to a composite representation where one expands in spherical-wave solutions within a sphere, and in plane waves in the region between the sphere and the cell boundary. The trial wave function which one obtains in a composite representation is clearly discontinuous, since even if one could match the two expansions on the surface of the sphere to all orders, the derivative of ψ would not in general be continuous across the boundary. In Appendix A of SM the following variational expression for the energy $\mathcal{E}_v$ suitable for trial functions discontinuous on a surface is discussed:

$$\mathcal{E}_v\int_\Omega d\Omega\,\psi^*\psi$$

$$=\int_{\Omega_i+\Omega_0} d\Omega\,\psi^*H\psi=\frac{1}{2}\int_S dS[(\partial_n\psi_0^*+\partial_n\psi_i^*)(\psi_0-\psi_i)$$

$$-(\psi_0^*+\psi_i^*)(\partial_n\psi_0-\partial_n\psi_i)] \tag{3a}$$

$$=\mathrm{Re}\left\{\int_{\Omega_i+\Omega_0} d\Omega\,\psi^*H\psi\right.$$

$$\left.+\int_S dS(\psi_0^*\partial_n\psi_i-\psi_i^*\partial_n\psi_0)\right\}, \tag{3b}$$

where ψ_i denotes the trial wave function in the inner region Ω_i, ψ_0 denotes the trial wave function in the outer region Ω_0, and S is the arbitrary boundary surface within the cell separating Ω_i and Ω_0. This expression is shown to yield eigenvalues correct to second order when the trial wave function has first-order errors. These eigenvalues are always real for any arbitrary trial wave function. Now applying Green's theorem to Ω_0 we find an equivalent variational expression:

$$\mathcal{E}_v\int_\Omega d\Omega\,\psi^*\psi$$

$$=\mathrm{Re}\left\{\int_{\Omega_i} d\Omega\,\psi^*\mathbf{H}\psi+\int_{\Omega_0} d\Omega(\boldsymbol{\nabla}\psi^*\cdot\boldsymbol{\nabla}\psi+\psi^*V\psi)\right.$$

$$\left.+\int_S dS(\psi_0^*-\psi_i^*)\partial_n\psi_0+\int_S dS\psi_0^*\partial_n\psi_i\right\}. \tag{3c}$$

We emphasize again that the variational expressions for the energy (3a)–(3c) hold for any trial wave function which is discontinuous on an arbitrary closed surface within the given domain.[5] We now make the particular choice of expanding the trial function ψ in N plane wave within Ω_0,

$$\psi_0(\mathbf{r},\mathbf{k})=\sum_{n=1}^{N}A_ne^{i\mathbf{k}_n\cdot\mathbf{r}}=\sum_{n=1}^{N}A_n\sum_{l=0}^{\infty}S_{nlir}(j_{lnr}/j_{lni}), \tag{4}$$

matched on a sphere of radius r_i centered about the nucleus to an expansion in L spherical wave solutions of the radial Schrödinger equation for energy ϵ_0 and potential $V(r)$,

$$\psi_i(\mathbf{k},\mathbf{r})=\sum_{n=1}^{N}A_n\sum_{l=0}^{L}S_{nlir}(R_{l\varepsilon_{0r}}/R_{l\varepsilon_{0i}}), \tag{5}$$

where $R_{l\varepsilon_{0r}}\equiv R_l(r,\mathcal{E}_0)$ is the solution of the radial equation for energy $\mathcal{E}_0$ regular at the origin;

$$R_l''+2R_l'/r+[\mathcal{E}_0-V(r)-l(l+1)/r^2]R_l=0. \tag{6}$$

$j_{lnr}\equiv j_l(k_nr)$ is the spherical Bessel function of order l, and $S_{nlir}=i^l(2l+1)j_{lni}P_l(\hat{k}_n\cdot\hat{r})$ is the expansion coefficient of $e^{(i\mathbf{k}_n\cdot\mathbf{r})}$ expanded in spherical waves.

Substituting (4), (5) into (3b) or (3c) and evaluating the various integrals we obtain a linear equation for $\mathcal{E}_v$ all terms of which are quadratic in the A_n, and A_n^*:

$$\mathrm{Re}\{\sum_{n,n'}A_n^*A_{n'}(H_{nn'}-\mathcal{E}_vD_{nn'})\}=0 \tag{7a}$$

As discussed in detail in Appendix B of SM, we can rewrite (7a) in terms of the real matrix elements $H_{nn'}{}^{(s)}$, where $H_{nn'}{}^{(s)}=\frac{1}{2}(H_{nn'}+H_{n'n})$, as follows:

$$\sum_{n,n'=1}^{N}A_n^*A_{n'}(H_{nn'}{}^{(s)}-\mathcal{E}_vD_{nn'})=0. \tag{7b}$$

Now differentiating (7b) with respect to A_n^* we are led

[10] The generalization from simple monatomic Bravais lattices to lattices with a basis is quite straightforward.

[11] Where we use atomic units in the equations, i.e., $\hbar=1$, energy in Ry, lengths in Bohr radii.

to a set of homogeneous linear equations for the A_n:

$$\sum_{n'=1}^{N} A_{n'}(H_{nn'}{}^{(s)}-\mathcal{E}_v D_{nn'})=0, \quad n=1 \text{ to } N \tag{8}$$

with the solution given by the vanishing of the secular determinant

$$|H_{nn'}{}^{(s)}-\mathcal{E}_v D_{nn'}|=0. \tag{9}$$

The matrix elements $H_{nn'}$, $H_{nn'}{}^{(s)}$ and $D_{nn'}$ are functions of $\mathcal{E}_0$. The explicit expression for $H_{nn'}{}^{(s)}$ which follows from (3c) is

$$H_{nn'}{}^{(s)}=\mathcal{E}_0 r_i{}^2\sum_{l=0}^{L} I_{l\mathcal{E}_0 i} b_{lnn'}+\Omega[(\mathbf{k}_n\cdot\mathbf{k}_{n'})\theta_{nn'}{}^0+V_{nn'}{}^0]$$
$$+r_i{}^2\sum_{l=0}^{L}\mathcal{L}_{l\mathcal{E}_0 i} b_{lnn'}+\tfrac{1}{2}r_i{}^2\sum_{l=L+1}^{\infty}(k_n j_{lni}'/j_{lni}$$
$$+k_{n'} j_{ln'i}'/j_{ln'i}) b_{lnn'}, \tag{10}$$

where

$$I_{l\mathcal{E}_0 i}\equiv\left(\int_0^{r_i} r^2 R_{l\mathcal{E}_0 r}{}^2 dr\right)\Big/ r_i{}^2 R_{l\mathcal{E}_0 i}{}^2$$
$$=-(\partial\mathcal{L}_{l\mathcal{E}_0 i}/\partial\mathcal{E}_0), \tag{11}$$

$$b_{lnn'}\equiv 4\pi(l+1) j_{lni} j_{ln'i} P_l(\hat{k}_n\cdot\hat{k}_{n'}), \tag{12}$$

$$\theta_{nn'}{}^0\equiv\Omega^{-1}\int_{\Omega_0} e^{i(\mathbf{k}_{n'}-\mathbf{k}_n)\cdot\mathbf{r}} d\Omega, \tag{13}$$

$$V_{nn'}{}^0\equiv\Omega^{-1}\int_{\Omega_0} V(r) e^{i(\mathbf{k}_{n'}-\mathbf{k}_n)\cdot\mathbf{r}} d\Omega, \tag{14}$$

$$\mathcal{L}_{l\mathcal{E}_0 i}\equiv R_{l\mathcal{E}_0 i}'/R_{l\mathcal{E}_0 i}, \tag{15}$$

and

$$j_{lni}'=[\partial j_l(k_n r)/\partial(k_n r)]_{r=r_i}. \tag{16}$$

The overlap matrix $D_{nn'}$ is given by

$$D_{nn'}=r_i{}^2\sum_{l=0}^{L} I_{l\mathcal{E}_0 i} b_{lnn'}+\Omega\theta_{nn'}{}^0. \tag{17}$$

We now note that the secular equation, (9), can be rewritten in terms of the matrix elements $D_{nn'}$ and $H_{nn'}{}^{(A)}$ which depend only on $\mathcal{E}_0$ and the lattice structure as

$$|H_{nn'}{}^{(A)}+(\mathcal{E}_0-\mathcal{E}_v)D_{nn'}|=0, \tag{18}$$

where

$$H_{nn'}{}^{(A)}=\Omega[(\mathbf{k}_n\cdot\mathbf{k}_{n'}-\mathcal{E}_0)\theta_{nn'}{}^0+V_{nn'}{}^0]$$
$$+r_i{}^2\sum_{l=0}^{L}\mathcal{L}_{l\mathcal{E}_0 i} b_{lnn'}$$
$$+\tfrac{1}{2}r_i{}^2\sum_{l=L+1}^{\infty}(k_n j_{lni}'/j_{lni}+k_{n'} j_{ln'i}'/j_{ln'i}). \tag{19}$$

If we set $\mathcal{E}_v=\mathcal{E}_0$ we arrive at the secular equation for the augmented-plane-wave (APW) method.[12] Retaining the term in $(\mathcal{E}_0-\mathcal{E}_v)D_{nn'}$ in the secular determinant we may use a rapidly convergent iterative procedure for solving this equation. This procedure greatly cuts down on the amount of computer time necessary to do a band calculation and is described in detail in Sec. II 4 of SM.

III. ENERGY-BAND STRUCTURE OF GOLD

The CWV method, described above, has been applied to mapping out the energy-band structure of Au in the nonrelativistic approximation. Calculations have been done at a large number of points in the Brillouin zone using an improved version of the computer programs utilized in our previous work.[1,13] The new programs were written in FORTRAN IV adapted to the CDC 6600 computer. The Fermi surface is mapped out and compared with the de Haas–van Alphen results of Schoenberg.[9]

A. Potential

The potential used in these calculations was constructed, by Sommers,[14] from the numerical Hartree-Fock solutions of the Dirac equation for the Au atom of Liberman, Waber, and Cromer.[7] The atomic Coulomb potential and the atomic charge density from eight shells of nearest neighbors were superposed with the atomic Coulomb potential and atomic charge density of the central atom, making use of the Lowdin α expansion,[15] to form the crystal Coulomb potential and charge density.[16] The crystal exchange potential was then calculated from the charge density using the Slater $\rho^{1/3}$ approximation. In the region between r_i and the outer boundaries of the cell, the potential was replaced by its average value.

B. Energy Bands

The computed curves of $\mathcal{E}(\mathbf{k})$ versus $\mathbf{k}$ in the principal symmetry directions in the fcc lattice are given in Figs. 1 and 2. The plot in Fig. 1 shows the conduction energy bands, which are close to the Fermi energy E_F while the excited states, which have energy higher than E_F, are plotted in Fig. 2.

For comparison, we have plotted in Fig. 3 the conduction energy bands for a potential constructed from the Liberman, Waber, and Cromer potentials, neglecting crystal exchange. We see when we compare Figs. 1

[12] J. C. Slater, Phys. Rev. **51**, 846 (1937).

[13] Listings of the FORTRAN II computer programs used in our previous work are given in the Ph.D. thesis of H. Schlosser, Physics Dept., Carnegie Institute of Technology, 1960 (unpublished).

[14] We wish to thank Dr. Sommers for supplying the crystal potential to us.

[15] P. O. Lowdin, Advan. Phys. **5**, 1 (1956).

[16] This procedure is discussed in detail in Chap. 3 of T. Loucks, *Augmented Plane Wave Methods* (W. A. Benjamin, Inc., New York, 1967).

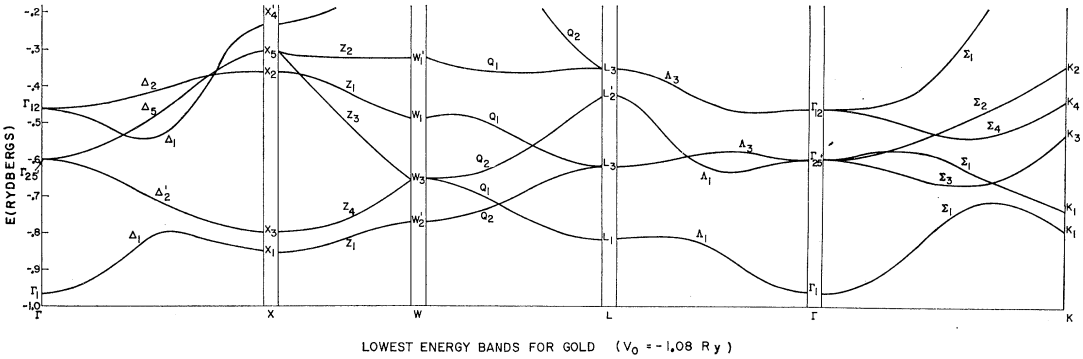

FIG. 1. Lowest energy bands of Au in the principal symmetry directions.

and 3 that the d-like bands are essentially unchanged in shape and energy with respect to V_0, when exchange is neglected, while the s- and p-like bands are considerably modified when exchange is included. Indeed at the L point the L_3 and L_2' are interchanged in order and hence the connectivity of the bands in the Q direction are modified. We find that when exchange is included the ordering of the levels at L is opposite to that found in Cu (Ref. 17) and Ag (Ref. 18). This will have a profound effect on the optical spectrum, and will be discussed in a later paper.

The energy eigenvalues for the conduction bands computed at a number of points in the zone are listed in Table I.[19] Several different slices of the sixth Brillouin zone are plotted in Figs. 4(a)–4(c), with the three constant energy contours corresponding to $\mathcal{E}=-0.25$, -0.28, and -0.30 Ry indicated. Figure 4(a) is a plot of the plane bounded by the symmetry points Γ-X-U-L-K, Fig. 4(b) is a plot of the plane bounded by the symmetry points Γ-X-W-K, while Fig. 4(c) is a plot of that part of a hexagonal face of the zone which is bounded by the symmetry points L-K-W-U.

C. Fermi-Surface Determination

In gold, one has a total of 11 electrons beyond the closed electron shells of the ion core. Now, since the first five Brillouin zones are completely filled and hence can accommodate ten electrons, the Fermi surface is defined as that constant energy surface in the sixth Brillouin zone which will just accommodate the eleventh electron. Hence, to fix the Fermi energy we must find that constant energy surface which encloses half the volume of the sixth zone. Equivalently, if we make explicit use of the zone symmetry we may concentrate on determining the volume of constant energy surfaces within the wedge-shaped region bounded by the planes defined by the symmetry points Γ-X-U-L, Γ-X-W-K, Γ-L-K, X-W-U, and L-K-W-U, and containing 1/48 of the zone volume.

In previous work, several different methods have been utilized for finding the volume of k space enclosed by a given constant energy surface. The first method consists of replacing the appropriate wedge-shaped region by a three-dimensional mesh of points, finding the energy eigenvalue at each mesh point, and then

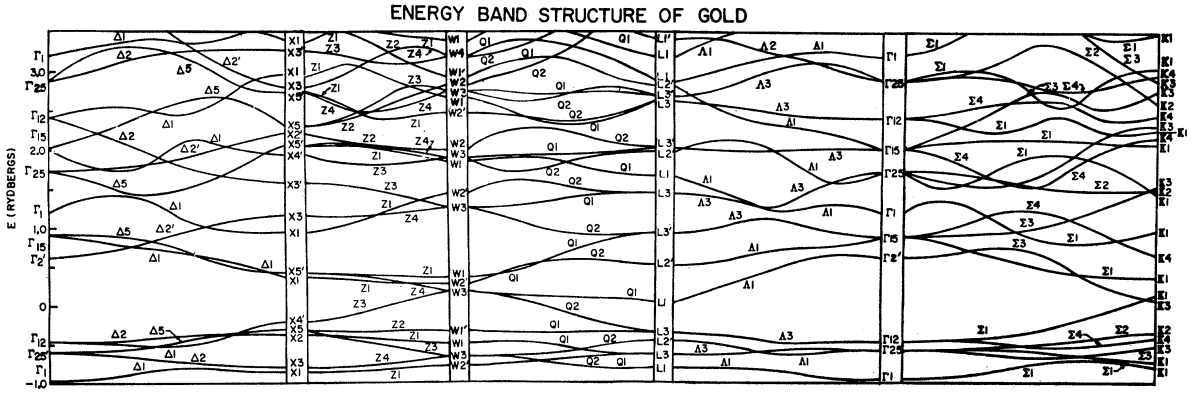

FIG. 2. Energy-band structure of Au in the principal symmetry directions.

[17] G. A. Burdick, Phys. Rev. **129**, 168 (1963); B. Segall, *ibid.* **125**, 109 (1962).
[18] J. Waber and E. Snow (private communication).
[19] Tables of the computed energy values for higher zones are available upon request from the author.

TABLE I. Energy (in Ry) versus reduced wave vector for conduction bands ($V_0 = -1.0826$ Ry).

	$\bar{k}_1$	$\bar{k}_2$	$\bar{k}_3$	Band 1	Band 2	Band 3	Band 4	Band 5	Band 6
Γ	0	0	0	1 −0.96866	25′ −0.60412	25′ −0.60412	25′ −0.60412	12 −0.46658	12 −0.46658
Δ	0.2	0	0	1 −0.93571	2′ −0.62644	5 −0.52216	5 −0.52216	1 −0.49293	2 −0.45744
Δ	0.4	0	0	1 −0.85420	2′ −0.68175	1 −0.54307	5 −0.52767	5 −0.52767	2 −0.43261
Δ	0.6	0	0	1 −0.80739	2′ −0.74054	1 −0.50914	5 −0.44324	5 −0.44324	2 −0.39993
Δ	0.8	0	0	1 −0.83436	2′ −0.78257	2 −0.37161	5 −0.35239	5 −0.35239	1 −0.34881
X	1.0	0	0	1 −0.85190	3 −0.79766	2 −0.36028	5 −0.30662	5 −0.30662	4′ −0.23713
Z	0.1667	1.0	0	1 −0.83457	4 −0.78227	3 −0.43219	1 −0.38709	2 −0.32220	3 −0.11398
Z	0.333	1.0	0	1 −0.79328	4 −0.73555	3 −0.55682	1 −0.44961	2 −0.32206	3 0.46564
W	0.5	1.0	0	2′ −0.76617	3 −0.65951	3 −0.65951	1 −0.48719	1′ −0.32198	3 0.19742
Q	0.5	0.125	0.875	2 −0.74669	1 −0.68418	2 −0.64012	1 −0.48550	1 −0.34971	2 0.08681
Q	0.5	0.25	0.75	1 −0.74086	2 −0.69802	2 −0.59056	1 −0.53594	1 −0.36520	2 −0.07949
Q	0.5	0.375	0.625	1 −0.79413	2 −0.64042	1 −0.59238	2 −0.51223	1 −0.35662	2 −0.2403
Λ	0.1	0.1	0.1	1 −0.94386	1 −0.61538	3 −0.52929	3 −0.52929	3 −0.47080	3 −0.47080
Λ	0.2	0.2	0.2	1 −0.87998	1 −0.63412	3 −0.57941	3 −0.57941	3 −0.46911	3 −0.46911
Λ	0.3	0.3	0.3	1 −0.82310	1 −0.60491	3 −0.58981	3 −0.58981	3 −0.42926	3 −0.42926
Λ	0.4	0.4	0.4	1 −0.81396	3 −0.60785	3 −0.60785	1 −0.50016	3 −0.37723	3 −0.37723
L	0.5	0.5	0.5	1 −0.81668	3 −0.61525	3 −0.61525	2′ −0.43015	3 −0.35376	3 −0.35376
Σ	0.15	0.15	0	1 −0.93184	3 −0.62292	2 −0.58982	1 −0.58629	4 −0.48566	1 −0.46119
Σ	0.3	0.3	0	1 −0.83813	3 −0.65820	1 −0.58411	2 −0.54935	4 −0.52151	1 −0.40596
Σ	0.45	0.45	0	1 −0.73594	3 −0.67015	1 −0.63751	4 −0.53751	2 −0.48993	1 −0.26588
Σ	0.6	0.6	0	1 −0.72164	1 −0.68372	3 −0.63496	4 −0.51325	2 −0.42360	1 −0.08803
K	0.75	0.75	0	1 −0.78866	1 −0.73123	3 −0.54567	4 −0.45023	2 −0.36544	1 0.11463
	0.6	0.6	0.3			O −0.57794	E −0.54415	O −0.361691	E −0.17777
	0.5	0.5	0.25	E −0.77829	E −0.63478	O −0.58726	E −0.55043	O −0.39830	E −0.2472
	0.4	0.4	0.2		E −0.6061	E −0.60381	O −0.58237	O −0.44499	E −0.33578
	0.3	0.3	0.15	E −0.8196	E −0.63832	E −0.58194	O −0.57267	O −0.48308	E −0.41161
	0.2	0.2	0.1	E −0.89870	E −0.6349	O −0.57887		O −0.48914	E −0.45459
	0.1	0.1	0.05	E −0.95044	E −0.6105	O −0.59561	E −0.59222	O −0.47350	E −0.46311
	0.2	0.1	0.1	E −0.9198	E −0.6195	E −0.58918	O −0.5710	E −0.48382	O −0.46153
	0.4	0.2	0.2	E −0.8289	E −0.6465	E −0.58923	O −0.5610	E −0.44864	O −0.41343
	0.5	0.25	0.25			E −0.60412		O −0.37643	E −0.37430
	0.6	0.3	0.3	E −0.7752	E −0.6493	E −0.58231	O −0.56575	O −0.35196	E −0.2705
	0.675	0.3375	0.3375			E −0.57634	O −0.56320	O −0.35045	E −0.1860
	0.75	0.375	0.375	E −0.7521	E −0.6697	E −0.56796	O −0.55777	O −0.36542	E −0.12347
	1.0	0.25	0.25		E −0.7806		E −0.54416	O −0.36435	E 0.0945
	0.8	0.2	0.2	O −0.7935	E −0.7455		E −0.53952	O −0.34142	E −0.12949
	0.7	0.175	0.175				E −0.5582	O −0.34846	E −0.25341
	0.6	0.15	0.15	E −0.7696	O −0.724		E −0.57912	O −0.37062	E −0.35822
	0.4	0.1	0.1	E −0.8394	O −0.6699		E −0.56811	E −0.49138	
	0.2	0.05	0.05	E −0.9285	E −0.6186	O −0.58400	E −0.58086	E −0.48755	O −0.45780
	0.2	0.1	0	E −0.9279	O −0.6184	O −0.58421	E −0.58122	E −0.48751	E −0.4550
	0.4	0.2	0	E −0.8278	O −0.6682		O −0.53060	E −0.50464	E −0.40296
	0.6	0.3	0	E −0.74843	O −0.7067	E −0.62841	E −0.46968	O −0.45044	E −0.26307
	0.8	0.4	0	E −0.7522	O −0.7008	E −0.63018	E −0.46541	O −0.36458	E −0.04081
	1.0	0.125	0.125				E −0.41484	O −0.37675	E −0.1311
	0.8	0.1	0.1				E −0.45709	O −0.34346	E −0.24092
	0.7	0.0875	0.0875					O −0.36354	E −0.33304
	0.6	0.075	0.075					E −0.41197	O −0.38759
	0.4	0.55	0.55				E −0.48163	O −0.43928	E −0.28196
	0.25	0.344	0.344				E −0.59099	E −0.39210	O −0.35624
	0.75	0.25	0.25				E −0.57648	O −0.34492	E −0.1396
	0.66	0.22	0.22				E −0.58950	O −0.34965	E −0.2558
	0.6	0.2	0.2					O −0.36175	
	0.6	0.45	0.45				E −0.48230	O −0.35619	E −0.28249
	0.55	0.4125	0.4125				E −0.48819	O −0.35313	E −0.30521
	0.5	0.375	0.375				E −0.51157	O −0.35992	E −0.33960
	0.9	0.3	0.3						E −0.03204
	0.8	0.35	0.35				E −0.58387	O −0.36881	E −0.06905
	0.675	0.4125	0.4125				E −0.52928	O −0.36014	E −0.20
	0.55	0.475	0.475					O −0.35463	E −0.32633
	0.45	0.525	0.525					O −0.35465	E −0.32558
	0.15	0.675	0.675						E −0.01706

counting the number of points properly weighted for symmetry, with energy less than the given energy. For the fcc structure of gold this entails knowledge of the energy eigenvalue at approximately 89 points within the wedge. An alternative approach was originally used by Segall for his calculations on Cu. It has the advantage of requiring knowledge of the energy eigenvalues at many fewer points in k space than method one. With the appropriate extensions, described below, this method is particularly appropriate for the noble metals. Segall recognized that near the Fermi surface, the constant energy surfaces in Cu, can be described in terms of an essentially spherical "belly" which swells out into eight "necks" near the various ⟨111⟩ directions

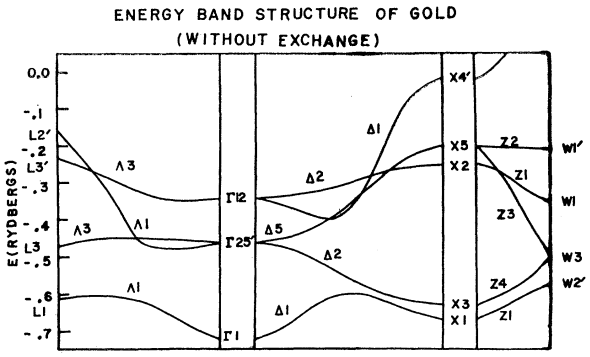

FIG. 3. Lowest energy bands of Au in the principal symmetry directions (no exchange included in crystal potential).

and contacts the zone boundary on the hexagonal faces of the zone. Thus to a good approximation, in Cu, the volume enclosed by any given constant energy surface, near the Fermi surface, equals the volume of the spherical belly plus the volume enclosed by the eight necks minus the volume of the eight spherical caps. The radius of the belly, in Cu, was taken by Segall to be equal to the mean of the ⟨100⟩ and ⟨110⟩ radii. Examination of Fig. 4(a) indicates that in the case of Au it would be a very poor approximation to replace the belly portions of the constant energy surfaces near the Fermi surface by spheres of radii equal to the mean of the ⟨100⟩ and ⟨110⟩ radii as Segall did for Cu. The reason for this is that the belly portions in Au are far from spherical. An inherently more accurate approximation to the volume of the belly can be obtained by making explicit use of the cubic symmetry of the crystal to obtain an appropriate average belly radius.[20] In this work we have combined Houston's method with Segall's procedure to fix the Fermi energy, as outlined below.

The basic idea of the Houston method is to express the average value of a quantity defined over a lattice with cubic symmetry in terms of its values along a finite set of symmetry directions in the lattice. For example, one can expand $\mathbf{k}^3(\mathcal{E},\omega)$ in a series of cubic harmonics,[21,22] $K_i(\omega)$, as follows:

$$\mathbf{k}^3(\mathcal{E},\omega)=\sum_{i=1}^{j} A_i(\mathcal{E})K_i(\omega)\,, \tag{20}$$

where ω is a direction cosine in the reciprocal lattice,

$$A_1(\mathcal{E})=1/4\pi\int \mathbf{k}^3(\mathcal{E},\omega)d\omega\equiv(\mathbf{k}^3)_{\rm av}\,, \tag{21a}$$

$$K_1=1\,, \tag{21b}$$

$$K_2=k_1{}^4+k_2{}^4+k_3{}^4-(3/5)k_4{}^4 \tag{21c}$$

$$K_3=(k_1k_2k_3)^2+(1/22)k^2K_2-(1/105)k^6\,, \tag{21d}$$

and

$$K_4=k_1{}^8+k_2{}^8+k_3{}^8-(28/5)k^2K_3 -(210/143)k^4K_2-(1/8)k^8\,. \tag{21e}$$

Now if one independently obtains $k^3(\mathcal{E},\omega)$ for a number of different symmetry directions in the reciprocal lattice, one can invert (20) and solve for $A_1(\omega)$. In this work we have made use of computed $\mathcal{E}$-versus-k curves in the Γ-X(100), Γ-K(110), Γ-W(210), 211, and 221 directions to obtain values of $\mathbf{k}^3(\mathcal{E},\omega)$ in the above five directions. Thus carrying out Houston's procedure outlined above, we obtain the following different

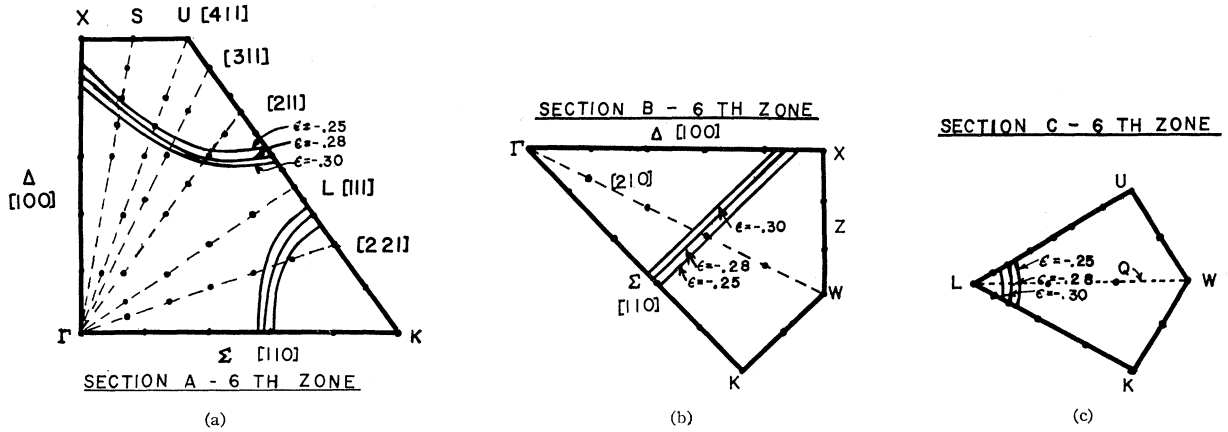

FIG. 4. (a) Slice of the sixth Brillouin zone of Au bounded by the symmetry points Γ-X-U-L-K with three constant energy contours. (b) Slice of the sixth Brillouin zone of Au bounded by the symmetry points Γ-X-W-K with three constant energy contours. (c) Portion of the hexagonal face of the sixth Brillouin zone of Au bounded by the symmetry points L-K-W-U with three constant energy contours.

[20] W. V. Houston, Rev. Mod. Phys. **20**, 161 (1948).
[21] F. von der Lage and H. Bethe, Phys. Rev. **71**, 612 (1947).
[22] D. D. Betts, A. B. Bhatia, and M. Wyman, Phys. Rev. **104**, 37 (1956).

approximations for $(\mathbf{k}^3)_{\rm av}$:

$$(\mathbf{k}^3)_{\rm av}{}^A=(4\pi/35)[7k^3([100])+10k^3([110])+18k^3([211])], \quad (22a)$$

$$(\mathbf{k}^3)_{\rm av}{}^B=(4\pi/560)[157k^3([100])+160k^3([110])+243k^3([221])], \quad (22b)$$

$$(\mathbf{k}^3)_{\rm av}{}^C=(4\pi/1400)[235k^3([100])+400k^3([110])+1008k^3([211])-243k^3([221])], \quad (22c)$$

$$(\mathbf{k}^3)_{\rm av}{}^D=(4\pi/3780)[531k^3([100])+680k^3([110])+625k^3([210])+1944k^3([211])], \quad (22d)$$

$$(\mathbf{k}^3)_{\rm av}{}^E=(4\pi/15120)[1089k^3([100])-1280k^3([110])+8750k^3([210])+656k^3([221])], \quad (22e)$$

where k^3 ([100]) denotes the value of $\mathbf{k}^3(\mathcal{E},\omega)$ in the [100] direction, etc.

In fixing the Fermi energy it is convenient to carry out the calculations in terms of the dimensionless reduced wave vector, $\bar{k}=\mathbf{k}a/2\pi$. Then the Fermi energy is given by the solution of

$$\bar{\Omega}(\mathcal{E}_F)=\int_{4\pi}\bar{k}_F{}^3(\omega,\mathcal{E}_F)d\omega+8[\bar{\Omega}_{\rm neck}(\bar{k}_F)-\bar{\Omega}_{\rm cap}(\bar{k}_F)]=6, \quad (23a)$$

or if we substitute (21a) in (23a) by

$$(\bar{k}_F{}^3(\mathcal{E}_F))_{\rm av}+2(\bar{\Omega}_{\rm neck}-\bar{\Omega}_{\rm cap})/\pi=6/4\pi=0.477417, \quad (23b)$$

where, $\bar{\Omega}$, $\bar{\Omega}_{\rm neck}$, and $\bar{\Omega}_{\rm cap}$ are the total volume enclosed by a given energy surface, the volume of a neck, and the volume of the spherical cap formed by the intersection of the belly and neck, respectively. The explicit procedure which we utilized to find $\bar{k}_F$ and hence $\mathcal{E}_F$ was to calculate the spherical average of the cube of the belly radius, $(\bar{k}_F{}^3(\mathcal{E}))_{\rm av}$, for the constant energy surface corresponding to $\mathcal{E}=-0.25$, -0.275, -0.29 Ry. This next enabled the calculation of the neck and spherical cap volumes. The results obtained for the three energies quoted above were $\bar{\Omega}/4\pi=0.47775$, 0.4130, 0.3843, respectively. Next, interpolating these results we find that the Fermi energy $\mathcal{E}_F=-0.2505\pm0.002$ Ry.

Using the result of the above Fermi energy determination we next obtained a number of the parameters of the Fermi surface. These results are present in Table II in terms of the free-electron reduced wave vector $\bar{k}_s=(3/2\pi)^{1/3}=0.782$. Comparison is made in the table with Roaf's[23] parametrization of the Fermi surface observed by Schoenberg using the de Haas–van Alphen effect. It can be seen from Table II that the belly of our calculated Fermi surface is somewhat more nonspherical than that obtained by Roaf; in addition, the neck radii which we found are larger than those of Roaf (i.e., the area of contact with the hexagonal face is greater in our calculation). The radius of contact of the neck with the hexagonal face is $\bar{k}/\bar{k}_s=0.211$. Finally it should be pointed out that with small adjustments in the crystal potential one could undoubtedly fit Shoenberg's Fermi surface. Presumably one could also achieve better agreement with the experiment by carrying out the band calculation to self-consistency. This was not done because of the magnitude of the extra effort involved in carrying a band calculation to self-consistency.

TABLE II. Radius vectors of the Fermi surface of gold as a function of polar angles (in units of $\bar{k}_s$).

	(*X*-*W*-*K*)		(*X*-*U*-*L*-*K*)	
θ/ϕ	HS[a] 0°	DR[b] 0°	HS[a] 45°	DR[b] 45°
0°	*X* 1.180	1.129	*X* 1.180	1.129
5°	1.092	1.103	1.092	1.103
10°	1.022	1.058	1.017	1.058
15°	0.971	1.020	0.985	1.021
20°	0.921	0.992	0.952	0.996
25°	0.883	0.972	0.933	0.984
30°	0.880	0.959	0.945	0.984
35°	0.845	0.950	0.965	0.996
40°	0.845	0.946	1.022	1.025
45°	*K* 0.845	0.945	1.120	1.092
50°	0.845	0.946	contact	contact
55°	0.845	0.950	contact	contact
60°	0.880	0.959	contact	contact
65°	0.883	0.972	contact	1.076
70°	0.921	0.992	0.953	1.014
75°	0.971	1.020	0.890	0.981
80°	1.022	1.058	0.869	0.960
85°	1.092	1.103	0.845	0.948
90°	*X* 1.180	1.129	*K* 0.845	0.945

[a] H. Schlosser, present work. [b] D. Roaf, Ref. 23.

ACKNOWLEDGMENT

The author wishes to acknowledge the aid and cooperation of the staff of the A.E.C. computing facility at the Courant Institute of Mathematical Sciences where the bulk of the numerical calculations were performed.

[23] D. J. Roaf, Phil. Trans. Roy. Soc. (London) **A255**, 135 (1963).